Dielectric relaxation and dielectric response mechanism in (Li, Ti)-doped NiO ceramics

2008 J. Phys.: Condens. Matter 20 395227

(http://iopscience.iop.org/0953-8984/20/39/395227)

J. Phys.: Condens. Matter **20** (2008) 395227 (11pp) doi:10.1088/0953-8984/20/39/395227

Dielectric relaxation and dielectric response mechanism in (Li, Ti)-doped NiO ceramics

Prasit Thongbai[1], **Suwat Tangwancharoen**[1], **Teerapon Yamwong**[2] **and Santi Maensiri**[1,3]

[1] Small & Strong Materials Group (SSMG), Department of Physics, Faculty of Science, Khon Kaen University, Khon Kaen 40002, Thailand
[2] National Metals and Materials Technology Center (MTEC), Thailand Science Park, Pathumthani 12120, Thailand

E-mail: sanmae@kku.ac.th and santimaensiri@gmail.com

Received 2 April 2008, in final form 5 August 2008
Published 4 September 2008
Online at stacks.iop.org/JPhysCM/20/395227

Abstract

Giant dielectric permittivity (Li, Ti)-doped NiO (LTNO) ceramics are prepared by a simple PVA sol–gel method. The dielectric properties are investigated as a function of frequency (10^2–10^6 Hz) at different temperatures (233–473 K). The concentration of Li has a remarkable effect on the dielectric properties of the LTNO ceramics. The modified Cole–Cole equation, including the conductivity term, is used to describe the experimental dielectric spectra of a high permittivity response with excellent agreement over a wide range of frequencies (10^3–10^6 Hz) and temperatures (233–313 K). A frequency dielectric dispersion phenomenon in an LTNO ceramic is also analyzed by impedance spectroscopy. A separation of the grain and grain boundary properties is achieved using an equivalent circuit model. The grain and grain boundary conduction and the dielectric relaxation time of the $Li_{0.05}Ti_{0.02}Ni_{0.93}O$ follows the Arrhenius law associated with estimated activation energies of 0.216, 0.369 and 0.391 eV, respectively. Through the analysis by the modified relaxation model and impedance spectroscopy, it is strongly believed that the high dielectric permittivity response of the LTNO is not only contributed by the space charge polarization (Maxwell–Wagner polarization) mechanism at low frequency regions, but also by the defect-dipole polarization mechanism at high frequency regions.

(Some figures in this article are in colour only in the electronic version)

1. Introduction

High permittivity Bi/Pb-free dielectric materials with good thermal stability have particularly attracted ever-increasing attention for their practical applications in microelectronics such as capacitors and memory devices. These materials include $CaCu_3Ti_4O_{12}$ (CCTO) [1], some Fe-containing complex perovskites $\mathbf{A}(Fe_{1/2}\mathbf{B}_{1/2})O_3$ (**A** = Ba, Sr, Ca and **B** = Nb, Ta, Sb) [2, 3], (**M**, **N**)-doped NiO (**M** = Li, Na, K and **N** = Ti, Al, Si, Ta) [4–10] and CCTO–LTNO composites [11]. They generally exhibit a very high and nearly temperature-independent dielectric permittivity at evaluated temperatures. Several models have been already proposed to explain the origin of high dielectric permittivity (high ε') in these compounds [12–15]. Nowadays, it is generally accepted that high ε' in CCTO ceramics are electrically heterogeneous consisting of semiconducting grains and insulating grain boundaries [16]. Therefore, high ε' in the CCTO is associated with an internal barrier layer capacitance (IBLC) effect due to the development of Schottky barriers at grain boundaries rather than being due to an intrinsic contribution. Hence, polarization effects at insulating grain boundaries between semiconducting grains or other internal barriers generate extrinsic high ε', accompanied by a strong Maxwell–Wagner (MW) relaxation mode. However, some fundamental questions regarding

[3] Author to whom any correspondence should be addressed.

the composition–property relationships remain unanswered. For example, what is the origin and composition of the semiconductive grain and insulating grain boundary in CCTO? For other high-ε' materials apart from CCTO, a grain boundary (internal) barrier layer capacitor has also been evoked to explain these high permittivity phenomena.

For nonperovskite materials (**M**, **N**)-doped NiO (**M** = Li, Na, K and **N** = Ti, Al, Si, Ta), it is now widely accepted that the high ε' at radio frequencies near room temperature is associated with the IBLC effect, arising from core/shell structure, which induces Maxwell–Wagner polarization (i.e. interfacial polarization) at the interfaces between grains (semiconducting/high conducting region) and grain boundaries (insulating/low conducting region) [4, 7, 17, 18]. The **N** dopant is rich on the grain boundaries (indigent within the grains) and forms a second phase, which acts as an insulator enclosing the core of the grain, which is semiconductive **M**-doped NiO particles, and the polarization relaxation is closely related to the conductivity in the grain interior [17]. Raevski *et al* [2] have suggested that the effective dielectric permittivity (ε') of the core/shell structure at very low frequency can be estimated as $\varepsilon' \approx \varepsilon_2(t+d)/d$, where ε_2 is the dielectric permittivity of the grain boundary (shell) and t and d are the size of the conducting grain (core) and the thickness of the shell, respectively. This relation is consistent with the experimental results, reported by Wu *et al* [4]. Namely, the dielectric permittivity of LTNO ceramics decreases with increasing Ti dopant (d increased). In contrast, Zhang *et al* [19] reported that high dielectric permittivity of an (Li, Ti)-doped NiO thin film with 200 nm in thickness increases with increasing Ti content. Moreover, Lin *et al* [18] have proposed that the huge dielectric permittivity response of $Li_xTi_yNi_{1-x-y}O$ (LTNO) could also be enhanced by the polarization of defect dipoles. Therefore, the Ti-dopant in LTNO ceramics and thin films may not only act as insulator, which restricts the long-range migration of charge carriers, but also contributes to the dielectric properties.

Unfortunately, only a few studies have focused on the defect-dipole polarization response of these materials to characterize relaxation processes, which are closely related to the formation of high permittivity in LTNO ceramics. Most recently, we reported that the polymerized complex (PC) method can be used to synthesize ∼39 nm nanoparticles of $Li_{0.3}Ti_{0.02}Ni_{0.68}O$ and to fabricate ceramics showing $\varepsilon' \sim 10^5$–10^6. However, the $Li_{0.3}Ti_{0.02}Ni_{0.68}O$ powders prepared by this method contained some second phase (i.e. Ni).

In this paper, a nonperovskite and nonferroelectric high permittivity core/shell structured materials, Li and Ti co-doped NiO ($Li_xTi_{0.02}Ni_{0.98-x}O$, where x = 0.05 0.10 and 0.20), are successfully synthesized by a simple polyvinyl alcohol (PVA) sol–gel method. The PVA sol–gel method is a chemical solution process, which has received considerable attention due to its relative simplicity and usefulness for obtaining a homogeneous and fine powder precursor [20]. The synthesized fine LTNO powders and ceramics are characterized by x-ray diffraction (XRD) and scanning electron microscopy (SEM). The high dielectric permittivity and its relaxation were investigated on the LTNO ceramics. It is suggested that such a high dielectric response of LTNO could be partially enhanced by the IBLC mechanism through MW relaxation at low frequency (<1 kHz), and partially associated with the polarization of defect dipoles above 1 kHz. Both contributing factors are thermally activated mechanisms.

2. Experimental details

$Ni(NO_3)_2{\cdot}6H_2O$ (99.9%, Kento), $LiNO_3$ (98%, Panreac), titanium(diisopropoxide) bis(2,4-pentanedionate) 75 wt% in 2-propanol ($C_{16}H_{28}O_6Ti$, Ti solution) (99%, Acros), citric acid ($C_6H_8O_7{\cdot}H_2O$, 99%, BDH) and polyvinyl alcohol (PVA) ($[-CH_2CHOH-]_n$, M_n = 72 000, Fluka) were employed as starting raw materials. The polycrystalline LTNO ceramic samples with different contents of Li, i.e. $Li_{0.05}Ti_{0.02}Ni_{0.93}O$ (LTNO-05), $Li_{0.10}Ti_{0.02}Ni_{0.88}O$ (LTNO-10) and $Li_{0.20}Ti_{0.02}Ni_{0.78}O$ (LTNO-20) were designed and prepared by the following procedure. Firstly, 5 g of citric acid was dissolved in 95 ml of distilled water (CA solution) with constant stirring using a magnetic stirrer at room temperature, and then 5 g of PVA was added to this solution by stirring at 473 K to obtain the polymer solution network. Secondly, stoichiometric amounts of $Ni(NO_3)_2{\cdot}6H_2O$ and $LiNO_3$ were added to this solution. Subsequently, Ti solution was slowly added into the mixed solution, followed by stirring and heating at 353 K to form the transparent gel. Note that the ratio of CA solution: PVA: total amount of the precursors is about 100:5:10 wt%. Then, the gel precursor was dried at 393 K overnight. To obtain the LTNO powders, the dried gel was ground and later calcined at 923 K for 10 h in air. The resulted powders were pressed into pellets 16 mm in diameter and ∼1–2 mm in thickness by a uniaxial pressing method at 200 MPa. Finally, these pellets were sintered at 1523 K for 5 h in air.

To reveal the phase composition and microstructure, the LTNO powders and ceramics were characterized by x-ray diffraction (XRD) (Philips PW3040, The Netherlands), energy-dispersive spectroscopy (EDS), and scanning electron microscopy (SEM) (LEO 1450VP, UK), respectively. The ceramic samples were polished and electroded by silver paint on both sides of the disc-shaped samples. They were allowed to dry overnight. The dielectric response of the samples was measured using a Hewlett Packard 4194A impedance gain phase analyzer over the frequency ranges from 100 Hz to 1 MHz and at the oscillation voltage of 1.0 V. The measurements were performed over the temperature ranges from 233 to 473 K using an inbuilt cooling–heating system. Each measured temperature was kept constant with an accuracy of ±1 K.

The complex impedance (Z^*) of the samples was calculated from the relation

$$\varepsilon^* = \varepsilon' - j\varepsilon'' = \frac{1}{j\omega C_0 Z^*} \tag{1}$$

where ε' and ε'', respectively, are the real part and imaginary part of the complex permittivity (ε^*). ω is the angular frequency ($\omega = 2\pi f$) and $j = \sqrt{-1}$. $C_0 = \varepsilon_0 S/d$ is the empty cell capacitance, where S is the sample area and d is the sample thickness. The values of ac conductivity (σ_{ac}) were derived from

$$\sigma_{ac} = \varepsilon_0 \omega \varepsilon''. \tag{2}$$

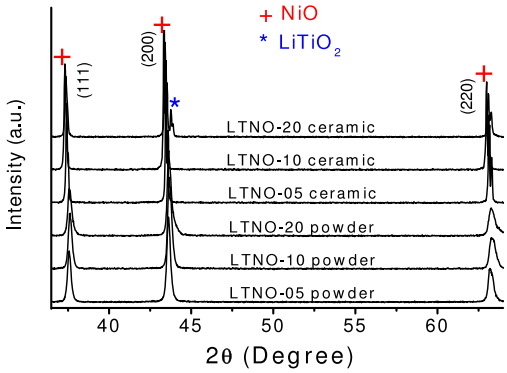

Figure 1. XRD patterns of LTNO powders and ceramics.

Table 1. Lattice parameter a and grain size of the LTNO ceramics.

Sample	Lattice parameter (Å)	Grain size (μm)
LTNO-05	4.165	6.29
LTNO-10	4.169	4.80
LTNO-20	4.164	6.99

3. Results and discussion

Figure 1 shows the XRD patterns of the LTNO powders and the sintered ceramics with different Li contents, confirming a possibility to produce the LTNO phase at a much lower reaction temperature compared to those prepared by the sol–gel route [4] and PC method [5]. All of the main peaks are comparable to those of the powder diffraction pattern of NiO in JCPDS card no. 78-0429 and those reported in the literature for cubic NiO [18, 21]. However, the second phase of $LiTiO_2$ is observed in the sintered LTNO-20 sample (JCPDS card no. 74-2257). The lattice parameters, determined from the diffraction patterns using Cohen's method, are summarized in table 1. These values are close to values reported in JCPDS card no. 78-0429 for cubic NiO with the lattice distortion of ∼0.05–0.3%. The SEM micrographs, shown in figure 2, reveal that the LTNO ceramics are dense and have obvious grain and grain boundary structure. The mean grain sizes are about 6.29±2.11, 4.8 ± 1.51 and 6.99 ± 2.28 μm for LTNO-05, LTNO-10 and LTNO-20, respectively.

Figure 3(a) shows a typical SEM image of the fracture surface of the LTNO-05 sample; labeled with numerals 1–3 are the EDS measurement points. The EDS spectrum at point 2 is shown in figure 3(b), confirming the presence of Ti dopant in the microstructure of our LTNO-05 sample. The results of the EDS measurements at the grain and grain boundary regions, shown in figure 3(c), indicate that the Ti component can be found in both the grain and grain boundary layer. However, the concentration of Ti content at the grain boundary (point 2) was higher than that in the grain (points 1 and 3).

The temperature dependence of the real part of the complex permittivity (ε') and dissipation factor ($\tan\delta = \varepsilon''/\varepsilon'$) of LTNO-05 is shown in figure 4(a) at selected frequencies between 0.5 and 500 kHz. ε' is nearly independent of temperature above a characteristic temperature, increasing

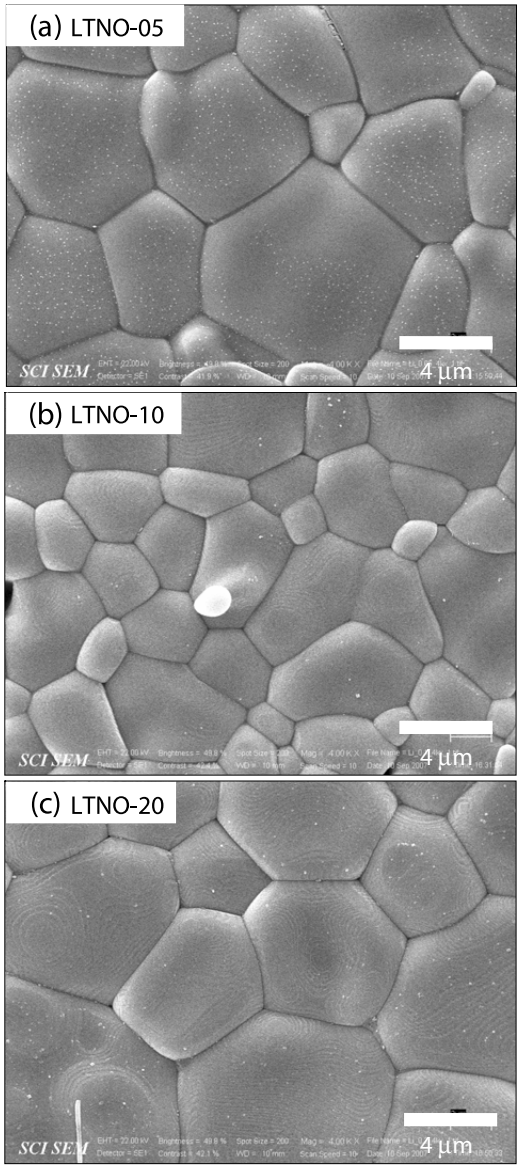

Figure 2. SEM micrographs of LTNO ceramics: (a) LTNO-05, (b) LTNO-10 and (c) LTNO-20.

with frequency increase. It attains a high value of $\varepsilon' \sim 10^4$, which is close to the value reported in [4] and much larger than that of pure NiO of ∼30 (at 1 kHz). The high ε' for LTNO is not related to the intrinsic nature of ferroelectricity (a thermally driven phase transition) [4]. Below the characteristic temperature, a rapid decrease of ε' by about two orders of magnitude is observed, being accompanied by the appearance of corresponding relaxation peaks in the $\tan\delta$. The peak shifts to lower temperature as the frequency decreases. This confirms the thermally activated behavior which is typical for the Maxwell–Wagner relaxation. At high temperature and low frequency, the increase in $\tan\delta$ may be attributed to the migration of excited electrical particles.

Figure 4(b) shows the temperature dependence of ε' and $\tan\delta$ for LTNO-05, LTNO-10 and LTNO-20 at 1 kHz. The ε' values at room temperature for the LTNO-05, LTNO-10 and LTNO-20 samples are 9063, 74499 and 128236,

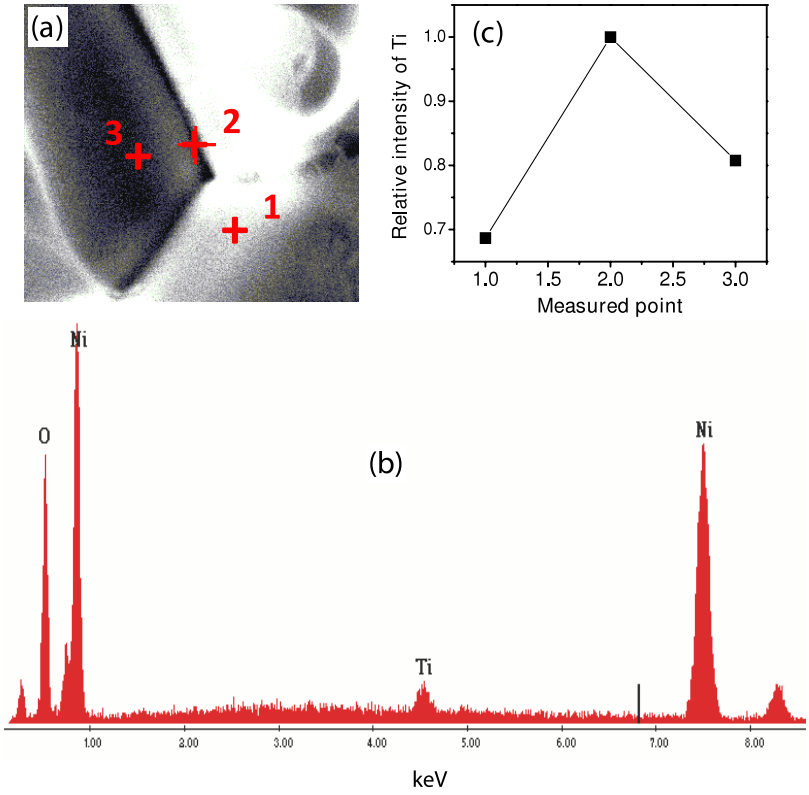

Figure 3. (a) SEM micrograph of the fractured surface of LTNO-05 sample, (b) EDS spectra at point 2 in (a) and (c) Ti element profile obtained from the EDS spectra.

respectively. The ε' value for the LTNO-20 sample is nearly 14 times larger than that for the LTNO-05 sample. It is well known that NiO is a Mott–Hubbard insulator at room temperature [22]. However, introduction of Ni^{2+} vacancies (V''_{Ni}) and/or doping with monovalent cation impurities like Li^{+} can dramatically increase the conductivity of NiO and thus NiO becomes semiconducting due to these defects [18]. Earlier works [4, 17] have shown that the Ti dopant is rich on the grain boundaries but indigent within the grains in (Li, Ti)-doped NiO ceramics. Thus the interiors of the grains for LTNO are semiconducting (i.e. Li-doped NiO), while the shells of the grains are Ti-rich insulating boundaries (e.g. $NiTiO_3$). The giant dielectric permittivity observed in our (Li, Ti)-doped NiO ceramics is therefore caused by its microstructure, because of the creation of an effective circuit of parallel capacitors, as found in boundary layer capacitors (BLC) [23]. According to the BLC structure and Maxwell–Wagner models, under an applied electric field the carrier conducting access is blocked by the Ti-rich boundary layer and thus the opposite charges will accumulate at the two edges of the insulator layer, creating a macroscopic electric dipole, which can be considered as a micro-parallel capacitor. As a result, the polarization formation primarily depends on the accumulation of charge via conduction in the grain interior. Therefore, an LTNO ceramic with higher Li concentration will possibly process more polarization and ascribe to the boundary layer capacitance effects. The highest dielectric permittivity seen in the LTNO-20 is therefore due to its higher Li concentration compared to those of the LTNO-10 and LTNO-05 samples. Note that, because the doping concentration of Ti is kept constant, the difference in dielectric behavior of LTNO samples can only be attributed to the effect of Li. As shown in figure 4(b), with the increase in temperature, the ε' values of LTNO-10 and LTNO-20 samples drop rapidly. This corresponds to the strong increases in their $\tan\delta$ values at the same temperature range. Such electrical responses of the LTNO-10 and LTNO-20 samples in the high temperature region may be attributed to the migration of excited electrical particles at high temperatures. However, the detailed description of the associated conduction behavior goes beyond the theme of this paper.

To understand the possible mechanism for high permittivity in LTNO-05, the real part (ε') and imaginary part (ε'') of the complex permittivity are plotted as a function of frequency over a temperature range of 233 and 313 K, as shown in figures 5(a) and (b). It is clear that ε' and ε'' show a Debye-like relaxation, namely ε' displaying a step decrease at the frequency and the relaxation peak shifting to higher frequency with increasing temperature. At high temperature, ε' increases in the low frequency range (<1 kHz), and with increasing frequency up to 10^4–10^5 Hz, a sharp decrease of ε' is observed. Normally, space charge (interfacial) polarization occurs when mobile charge carriers are impeded by a physical barrier (i.e. grain boundary) that inhibits charge migration. The charges then pile up at the barrier, producing a localized polarization within grains [24]. With increased temperature, the density of charges contributing to the space charge polarization is sufficiently large. The frequency range of sensitivity for such polarization may extend from 10^{-3} Hz into the kilocycle range,

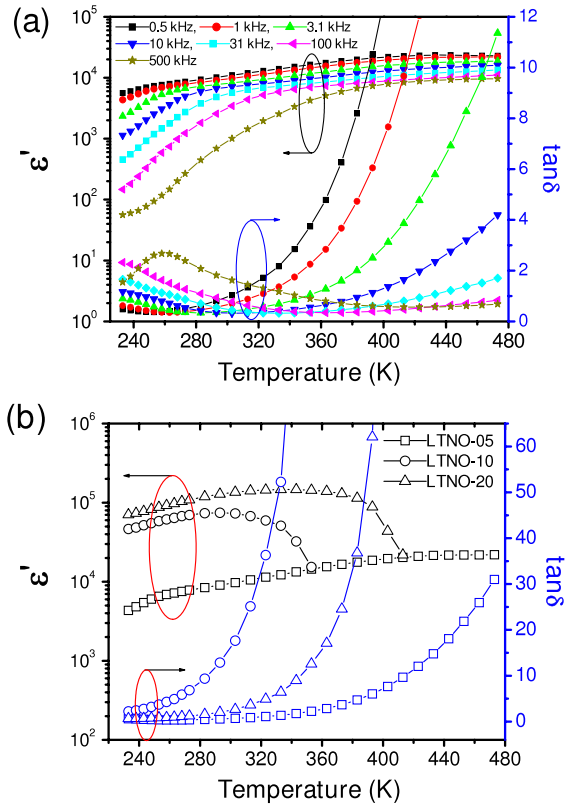

Figure 4. (a) Temperature dependences of ε' and $\tan\delta$ for LTNO-05 at selected frequencies and (b) the temperature dependence of ε' and $\tan\delta$ for LTNO-05, LTNO-10 and LTNO-20 at 1 kHz.

producing a very large ε' in this region. Therefore, the increase in ε' at low frequency is possibly due to space charge polarization. For the step-like decrease in ε' at the frequency range of 10^3–10^5 Hz (corresponding to the respective relaxation peaks in ε'') as shown in figure 5(b), dielectric relaxation in this region may be ascribed to the defect-dipole polarization effect, which appears at radio-frequency ranges. In general, there are two main effects responsible for the mechanism of polarization: the frequency of applied electric field and temperature. According to the effect of frequency, at fixed temperature, if an alternating field is applied then the polarization may fully develop at sufficiently low applied frequencies (the polarization and the field are in phase) but if the frequency of the applied field is too high then the field is reversed before the polarization has responded and no response will be the result of the net effect. The magnitude of the polarization thus drops off as the frequency is increased. For the effect of temperature [7], at low temperature, the electric dipoles freeze through the relaxation process, and there exists decay in polarization with respect to the applied electric field, which results in the sharp decrease in ε'. When the temperature is high, the rate of polarization formed is quick, and thus the relaxation occurs in high frequency as shown in figure 5(a).

In general, the frequency-dependent behavior of ε' and ε'' of high dielectric permittivity can be well described by the simple Cole–Cole relaxation equation, which ignores the effect of the electrical conduction [25, 26]:

$$\varepsilon^* = \varepsilon' - \mathrm{j}\varepsilon'', \tag{3}$$

$$\varepsilon^* = \varepsilon_\infty + \frac{\varepsilon_s - \varepsilon_\infty}{1 + (\mathrm{j}\omega\tau)^{1-\alpha}}, \tag{4}$$

where ε_s and ε_∞ are respectively, the static and high frequency limits of dielectric permittivity, τ is the most probable relaxation time and α is the Cole–Cole parameter with values between 0 and 1. For an ideal Debye relaxation, $\alpha = 0$. If $\alpha > 0$, it implies that the relaxation has a distribution of relaxation times, leading to a broader peak shape than a Debye peak. However, when the electrical conductivity is dominated at the low frequency range as shown in figures 5(a) and (b), a contribution term by electrical conduction is generally added to the relaxation equation. The modified Cole–Cole equation that incorporates the conductivity term is given by [3, 27]

$$\varepsilon^* = \varepsilon_\infty + \frac{\varepsilon_s - \varepsilon_\infty}{1 + (\mathrm{j}\omega\tau)^{1-\alpha}} - \mathrm{j}\frac{\sigma^*}{\varepsilon_0\omega^s} \tag{5}$$

where $\sigma^*(\sigma^* = \sigma_1 + \mathrm{j}\sigma_2)$ is the complex conductivity. Here σ_1 is the conductivity due to the free charge carrier (dc conductivity) and σ_2 is the conductivity due to the space charges (localized charges) and s is a dimensionless exponent $(0 < s < 1)$. For an ideal complex conductivity, $s = 1$. If $s < 1$, it implies that the polarization has a distribution of the carrier polarization mechanism. From this relation, the complex permittivity can be decomposed into the real and imaginary parts. i.e.

$$\varepsilon' = \varepsilon_\infty + \frac{(\varepsilon_s - \varepsilon_\infty)\left\{1 + (\omega\tau)^{1-\alpha}\sin(\alpha\pi/2)\right\}}{1 + 2(\omega\tau)^{1-\alpha}\sin(\alpha\pi/2) + (\omega\tau)^{2-2\alpha}} + \frac{\sigma_2}{\varepsilon_0\omega^s}, \tag{6}$$

and

$$\varepsilon'' = \frac{(\varepsilon_s - \varepsilon_\infty)(\omega\tau)^{1-\alpha}\cos(\alpha\pi/2)}{1 + 2(\omega\tau)^{1-\alpha}\sin(\alpha\pi/2) + (\omega\tau)^{2-2\alpha}} + \frac{\sigma_1}{\varepsilon_0\omega^s}. \tag{7}$$

It is clearly seen from equations (6) and (7) that the conductivity may have contributions to the dielectric permittivity (ε') and dielectric loss (ε''). The first term of equation (7) is the part of the losses associated with the dielectric relaxation due to permanent dipole orientation or other motions which do not involve long-range displacement of mobile charge carriers, whereas the second term is the part of the losses associated with long-range migration of carrier response. From the above equations, the charge carrier localization at defect sites and interfaces (σ_2) can make a large contribution to the dielectric permittivity, while the free charge carrier (σ_1) contributes to the dielectric loss.

Analysis of the experimental data was carried out on the basis of equations (6) and (7). Typical fitting results are shown in figures 5(a) and (b): the solid lines are the fitted curves of experimental results. As clearly seen from figures 5(a) and (b), the excellent agreement between experimental data and calculated data over the entire range of frequencies and temperatures for both ε' and ε'' is consistent with equations (6) and (7) for LTNO-05 ceramic. We notice a disagreement between the measured and calculated values for ε' at low

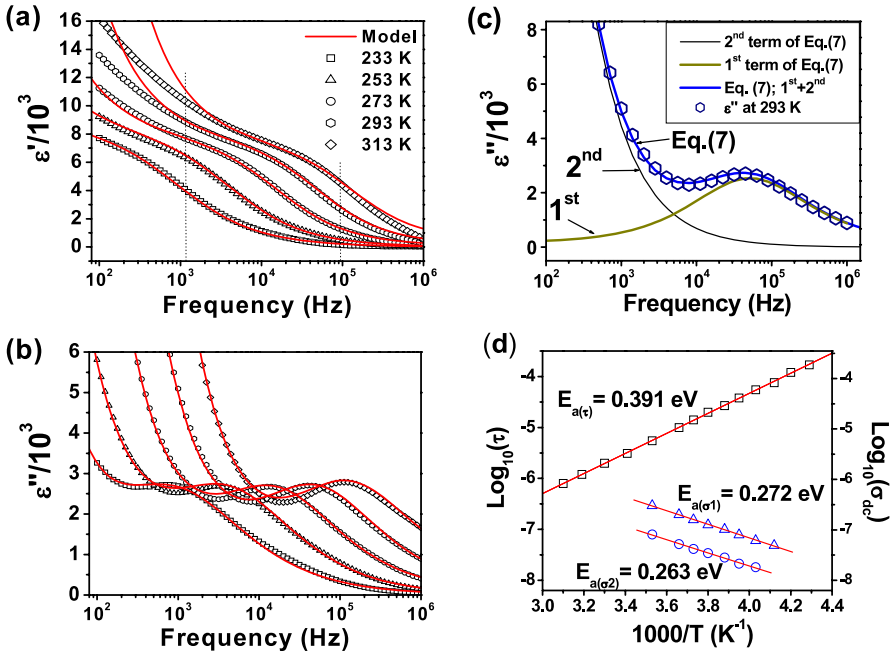

Figure 5. Frequency dependences of ε' (a) and ε'' (b) of LTNO-05 at various temperatures. The solid curves are the best fits to equations (6) and (7) for ε' (a) and ε'' (b), respectively, which include both a Cole–Cole relaxation and a complex conductivity contribution. (c). The evolution of the relaxation and dc conductivity contribute to the dielectric loss. (d) Arrhenius plots of the relaxation time and dc conductivities.

frequencies (<1 kHz) at temperature above 273 K. This may be due to the fact that some parts of the Ti dopant have entered into the NiO crystal lattice [17] and have an influence on the space charge localized inside the grain. Additionally, figure 5(c) shows the evolution of the relaxation and dc conductivity contributing on dielectric loss at 293 K. It is clearly seen that there are two main factors responsible for the dielectric relaxation of LTNO: dipole and conduction relaxation. A complete list of parameters used in the calculation ($\Delta\varepsilon(\varepsilon_s - \varepsilon_\infty)$, τ, α, s, σ_1 and σ_2) for LTNO-05 is shown in table 2. It is also important to mention that the s values tend to increase ($s \rightarrow 1$) with increasing temperature (does not present), indicating that the carrier polarization mechanism is weakly dispersive at higher temperature, which might be attributed to some barrier height extracted. For the value of α, a relatively lower value of $1-\alpha$ corresponds to a more disordered system. Hence it can be inferred from the $1-\alpha$ values of LTNO-05 (0.66) and CCTO (0.91) [28] at 233 K that a relatively higher disorder is present in LTNO-05 compared to that of the CCTO system.

In order to elucidate the dielectric relaxation response in LTNO-05, it is important to estimate the activation energy of relaxations. Figure 5(d) shows the plot of log τ with $1/T$, in which the solid line is the fitted result obeying the Arrhenius law:

$$\tau = \tau_0 \exp\left(\frac{E_{a(\tau)}}{k_B T}\right), \tag{8}$$

where τ_0 is the relaxation time at an infinite temperature, $E_{a(\tau)}$ is the activation energy for the relaxation, k_B is the Boltzmann constant and T is the absolute temperature. As shown in table 2 and figure 5(d), the rapid decrease in τ with increasing

Table 2. Fitted results of $\Delta\varepsilon(\varepsilon_s - \varepsilon_\infty)$, τ, α, s, σ_1 and σ_2 using the experimental results with equations (6) and (7) in a different temperature range for the LTNO-05.

T (K)	$\Delta\varepsilon = (\varepsilon_s - \varepsilon_\infty)$	α	s	τ (μs)	σ_1 (10^{-4} S m^{-1})	σ_2 (10^{-4} S m^{-1})
233	8700	0.340	—	170	—	—
253	8250	0.320	0.8	38	0.080	0.021
273	7800	0.300	0.8	10	0.210	0.053
293	7500	0.280	0.8	3.1	0.460	0.180
313	7000	0.275	0.85	1.2	1.350	0.640

temperature is suggestive of an increased dipole density and faster polarization process [4]. According to the fitted curve for the LTNO-05 sample, the activation energy $E_{a(\tau)}$ value of the relaxation process is 0.391 eV and $\tau_0 = 6.35 \times 10^{-13}$ s. Additionally, the value of $E_{a(\tau)}$ is higher than that of 0.313 eV as reported by Wu *et al*, for $Li_{0.05}Ti_{0.02}Ni_{0.93}O$ [4]. It is important to note that, with increasing Li concentration, the relaxation peak moves out of the measured frequency range, which is similar to that reported by Wu *et al* [4]. Thus, the $E_{a(\tau)}$ values of the LTNO-10 and LTNO-20 samples could not be obtained.

As previously mentioned, the addition of Li_2O to NiO leads to an increase in conductivity, and some defects can be introduced due to different valences of doped ions. For every added Li^+, one Ni^{2+} is promoted to the Ni^{3+} state, which is the lost electron filling a state in the oxygen 2p valence band. The lattice now contains Ni^{2+} and Ni^{3+} ions on equivalent sites and is the model situation for conduction by polaron hopping [29]. In the polaronic scenario, the nearest-neighbor hopping obeys

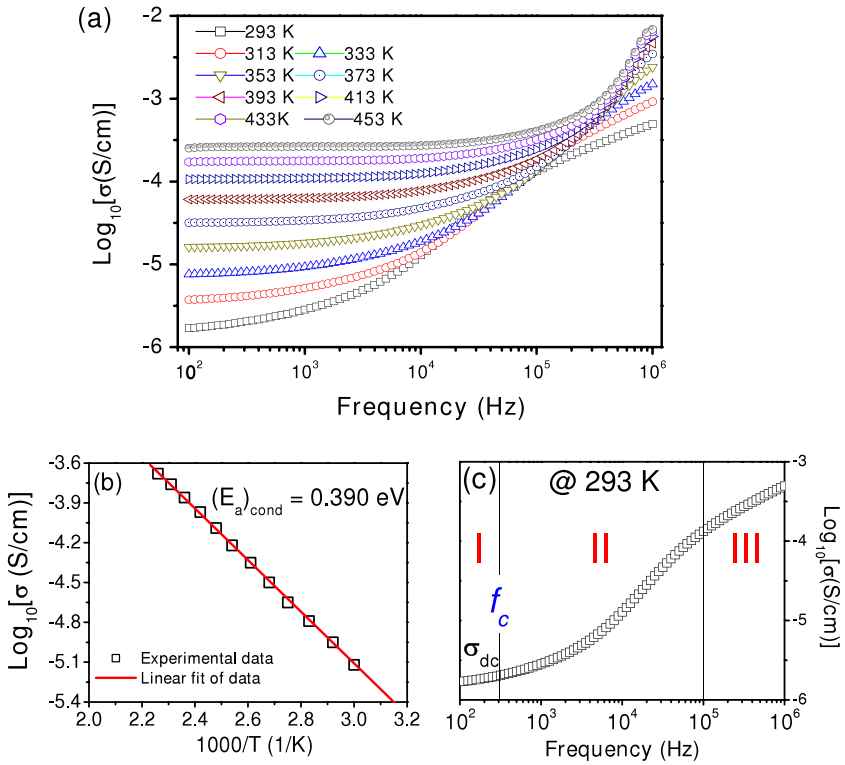

Figure 6. (a) Frequency dependence of ac conductivity at various temperatures. (b) Arrhenius plots of the temperature dependence of dc conductivity and (c) shows a typical conductivity spectrum of LTNO-05 ceramic at 293 K.

the Arrhenius-like law [30]

$$\sigma = \sigma_1' \exp\left(\frac{-E_{a(\sigma)}}{k_B T}\right), \tag{9}$$

where σ_1' is a constant and $E_{a(\sigma)}$ is the conduction activation energy. As shown in figure 5(d), we found that the fitted σ_1 and σ_2 values at different temperatures follow the Arrhenius-like law, in which the solid line is the fitted result. Accordingly, in the LTNO-05 sample, both of the conduction activation energies for the localized charge and free charge carrier, $E_{a(\sigma 2)} = 0.263$ eV and $E_{a(\sigma 1)} = 0.272$ eV, were obtained, respectively. As previously reported [4, 17], the polarization relaxation has a close relation to the conductivity in the grain interior, because the value of $E_{a(\sigma)}$ is almost the same as the value for $E_{a(\tau)}$. However, both values are different from our experimental results, indicating that the dielectric relaxation response in an LTNO-05 ceramic does not correspond to the conductivity in the grain interior.

In order to understand the effect of the conductivity on the dielectric properties of LTNO-05 ceramic, the frequency dependence of ac conductivity (σ_{ac}) was further characterized over the temperature from 293 to 453 K. As shown in figure 6, the σ_{ac} shows a dispersion that shifts to higher frequency with increasing temperature, and it decreases with decreasing frequency, and then it nearly saturates to a constant value at low frequency. Extrapolating these curves at low frequencies gives the dc conductivity (σ_{dc}). As illustrated in figure 6(c), the frequency dependence of ac conductivity at 293 K, a typical conductivity–frequency spectrum is divided into three parts [31]. In region I, according to the jump relaxation model, since at low frequency and/or at high temperature the electric field cannot perturb the hopping conduction mechanism of charged particles, the conductance is approximately equal to the dc value and the conduction mechanism is the same as that for dc conduction as mentioned above, i.e. hopping of charged particles from one localized site to another. The conductivity begins to increase nonlinearly after the frequency exceeds the critical frequency f_c in region II due to the fact that the capacitor admittance becomes numerically larger than the resistor admittance with increasing frequency. In region III, conductivity becomes proportional to frequency, resulting in nearly constant loss (NCL). In most materials, the NCL regime dominates the ac conductivity at high frequency or low temperature [32]. Here, we are interested in only region I (dc conducting region), but detailed descriptions of the associated conduction behavior in regions I and II go beyond the theme of this paper. As shown in figure 6(b), the resulting σ_{dc} follows an Arrhenius-like law in equation (9) with the estimated conduction activation energy of $E_{a(cond)} = 0.390$ eV. From this result, it is seen that the activation energy required for the relaxation ($E_{a(\tau)} = 0.391$ eV) is almost the same value as the activation energy required for hopping of charged particles. However, it is premature to associate the polarization relaxation with the conductivity because the activation energies of the two processes were carried out at different temperature ranges.

In order to clarify the observed behavior as mentioned above, we used impedance spectroscopy (IS) analysis to study the electrical behavior of LTNO-05 ceramic. Conventionally,

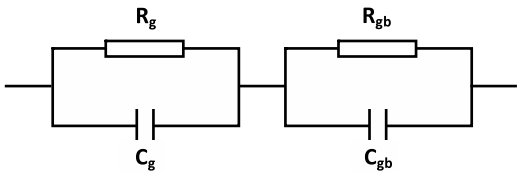

Figure 7. Equivalent circuit used to represent the electrical properties of a ceramic sample that exhibits grain (R_g, C_g) and grain boundary (R_{gb}, C_{gb}) effects.

the bulk and grain boundary contributions to the overall impedance can be resolved by exploiting differences in their responses to an alternating applied field. Separation of the bulk and grain boundary of the material is obtained by fitting the experimental response to that of an equivalent circuit, which is usually considered to comprise a series of parallel resistor–capacitor (R–C) elements, as shown in figure 7. The circuit consists of a series array of two subcircuits, one represents grain effects and the other represents grain boundaries. Each subcircuit is composed of a resistor and capacitor joined in parallel. Let (R_g, R_{gb}) and (C_g, C_{gb}) be the resistances and capacitances of grains and grain boundaries, respectively, then the impedance Z^* for the equivalent circuit in this system is [15]

$$Z^* = \frac{1}{R_g^{-1} + j\omega C_g} + \frac{1}{R_{gb}^{-1} + j\omega C_{gb}} = Z' - jZ'', \qquad (10)$$

where

$$Z' = \frac{R_g}{1 + (\omega R_g C_g)^2} + \frac{R_{gb}}{1 + (\omega R_{gb} C_{gb})^2} \qquad (11)$$

and

$$Z'' = R_g \left[\frac{\omega R_g C_g}{1 + (\omega R_g C_g)^2}\right] + R_{gb}\left[\frac{\omega R_{gb} C_{gb}}{1 + (\omega R_{gb} C_g b)^2}\right], \qquad (12)$$

where Z' and Z'' are the real and imaginary parts of complex impedance. Figure 8(a) shows the frequency dependence of Z'' at different temperatures. As shown in figure 8(b), at 233 K, a weak peak at about 500 kHz shifts to higher frequency with decreased intensity as the temperature increases, and it moves out of the frequency range of our experiment. However, with the temperature increased above 273 K, a strong peak appears in the measured frequency range as shown in figure 8(a), which also moves to higher frequencies with a fall in intensity as temperature increases. This implies that both electrical responses are thermally activated. Based on equation (12), the response peaks of the grains and grain boundaries are positioned at $1/(2\pi R_g C_g)$ and $1/(2\pi R_{gb} C_{gb})$, respectively, and the peak values are proportional to associated resistances. In general, the peak frequency for grain boundaries is much lower than that for grains due to their large resistance and capacitance compared with those of grains [12].

Figure 8(c) shows the impedance spectra for the LTNO-05 ceramic at various temperatures. It can be seen that the impedance semicircles became smaller with increasing temperature, and two semicircles were observed and overlapped according to figure 8(d). The appearance of two semicircles strongly suggests that the core–shell model is appropriate for further characterization. Therefore, in the impedance spectra, we attribute the small semicircle at high frequency, which corresponds to the weak peaks in figure 8(b), to the grains, whereas we attribute the big semicircle at low frequency, which corresponds to the strong peaks in figure 8(a), to grain boundaries.

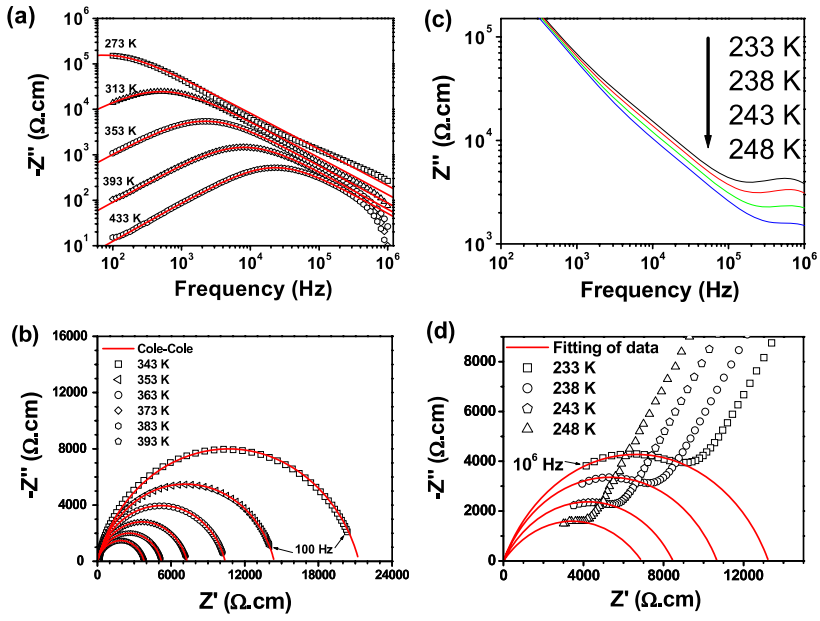

Figure 8. (a) Frequency dependence of the imaginary part (Z'') of impedance Z^* at high temperatures and the solid curves are the best fits to equation (14). (b) Frequency dependence of Z'' at low temperatures. (c) Impedance spectra as a function of temperature and the solid curves are the best fits to equation (14). (d) Impedance plane plot at low temperatures.

Table 3. Capacitances and conduction activation energies of grain and grain boundary of the LTNO samples.

	Capacitance (nF)		Resistance (Ω)		Conduction activation energy (eV)	
Sample	C_g (233 K)	C_{gb} (303 K)	R_g (233 K)	R_{gb} (303 K)	E_g	E_{gb}
LTNO-05	0.023	5.0	1.32×10^4	1.01×10^5	0.216	0.369
LTNO-10	—	17.0	99	0.25×10^3	—	0.302
LTNO-20	—	60.0	44	1.16×10^3	—	0.307

As shown in figure 8(a), it is appropriate to fit the Z'' to a single $R_{gb}C_{gb}$ parallel circuit due to the fact that the response peaks of the grains are too weak to be analyzed by equation (12), and it already moved out of the measured frequency range. Hence, equation (12) has been reduced to

$$Z^* = \frac{R_{gb}}{1 + j\omega R_{gb}C_{gb}}. \quad (13)$$

Unfortunately, equation (13) cannot be used to describe the experimental data very well. However, we found that the complex plane plot of Z^* is better described by using the Cole–Cole equation [25, 26], which is commonly used for polycrystalline ceramic samples [15]:

$$Z^* = \frac{R_{gb}}{1 + (j\omega\tau_{gb})^{1-\alpha}}, \quad (14)$$

where $\tau_{gb} = R_{gb}C_{gb}$ and the parameter α is constant ($0 < \alpha \leqslant 1$). By fitting the experimental data to equation (14), we obtained the values of R_{gb}, C_{gb} and α at different temperatures. The fitted values of α at different temperatures are in the range of 0.21–0.14. The value of α appears to decrease with increasing temperature. R_{gb} decreases from 1.5×10^6 Ω at 253 K to 1.1×10^3 Ω at 443 K, whereas $C_{gb} = 5$ nF is almost constant over the temperature range of 253 and 443 K. As shown in figure 8(d), the electrical response of the grain dominated at low temperatures, and the R_g and C_g values can simply be estimated by the relation that is similar to equation (14), i.e. $Z^* = R_g/[1 + (j\omega R_g C_g)^{1-\beta}]$. The fitted values of R_g and C_g are tabulated in table 3.

Conductivity data, σ, where $\sigma = R^{-1}$, were obtained from the fitted R_g and R_{gb} values for the bulk (σ_g) and grain boundary (σ_{gb}) components, and plotted against reciprocal temperature in Arrhenius format, in which the solid lines are the fitted results using equation (9). It is clearly seen from figure 9 that both are well fitted with the Arrhenius-like law. From the slopes of the fitted straight lines, we obtain an activation energy of about 0.369 eV for grain boundary and about 0.216 eV for grain, which indicate that the grain and grain boundary have different electrical transport characteristics. As previously reported, in the intermediate temperature range, heavy doping (5–10%) of Li in NiO induces a drop in activation energy from 0.9 eV to about 0.18 eV below 500 K [33]. It should be noted that the activation energy of the conductivity in the grain interiors for our LTNO-05 sample is about 0.216 eV, which is higher than 0.18 eV as

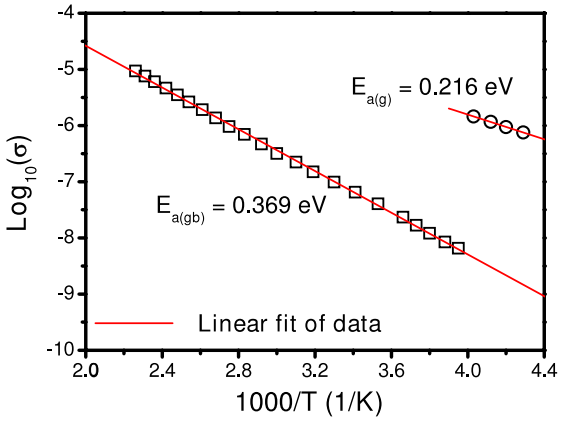

Figure 9. The Arrhenius plots of the conductivities of the grain and the grain boundary.

mentioned above. This is due to the fact that some part of Ti is incorporated into the crystal lattice of NiO and some defects are formed [17]. These results have an effect on the electric conductivity in the grains. Note that the value of grain conductivity activation energy in our LTNO sample is lower than that of the LTNO sample prepared by the sol–gel method, $E_{a(g)} = 0.309$ eV, reported by Wu *et al* [4]. This may be attributed to the difference in the concentration of the part of the Ti dopant that has entered into the grain interiors due to the difference in the preparation method. In our case, such a part of the Ti dopant may have a low concentration inside the grain. This implies that the distribution of Ti dopant in the LTNO microstructure is the only factor that has an impact on the electrical properties of the bulk LTNO ceramics. It is of special interest to note that the activation energy of the conductivity in the grain interiors ($E_{a(g)} \sim 0.216$ eV (figure 9)) is significantly lower than the activation energy required for relaxation ($E_{a(\tau)} \sim 0.391$ eV (figure 5(c))) as reported in the literature [7, 17]. In contrast, the value of activation energy for relaxation processes (∼0.391 eV) is close to the activation energy of the conductivity in a grain boundary (∼0.369 eV). However, it is premature to associate the high relaxation activation energy of the LTNO-05 sample with its grain boundary conductivity activation energy because there are several factors that have a strong effect on the electrical properties of the LTNO ceramics, such as the defects (vacancies) and internal domain within the grain. This implies that high dielectric response in the LTNO ceramics is not only contributed by the dc conductivity in the grain interiors, but also by the defect dipoles.

It is widely accepted that the giant dielectric permittivity in LTNO is extrinsic in origin, which can be attributed to a Maxwell–Wagner relaxation mechanism in material, and often arises in a material consisting of conductive grains separated by insulating grain boundaries (or other insulating interfaces) [12, 14]. Based on the Maxwell–Wagner relaxation model, the measured ultrahigh dielectric permittivity and the relaxation process in the complex permittivity as a function of frequency can be easily understood. However, it is only a simplified model of interfacial polarization based on an equivalent circuit, and does not provide a physical explanation

for the underlying polarization. Lin *et al* [18] used positron annihilation spectroscopy to investigate defect properties in LTNO and revealed that a large amount of defects exists in the LTNO ceramics. Some defects can be introduced due to the different valence of doped ions. This may be represented by the reaction [18]

$$Li_2O \xrightarrow{NiO} 2Li'_{Ni} + V_O^{\bullet\bullet} + O_\circ^x \quad (15)$$

$$TiO_2 \xrightarrow{NiO} Ti_{Ni}^{\bullet\bullet} + V''_{Ni} + 2O_\circ^x. \quad (16)$$

It is well known that NiO is p-dopable [34]. At room temperature, free-hole density is low in pure NiO, because the acceptor levels of the hole producer V_{Ni} are not close enough to the valence band maximum to ionize most vacancies. In other words, the free-hole density of cation-deficient of NiO is limited by a too large an ionization energy of the Ni vacancy. However, it can be strongly increased by extrinsic dopants (e.g. Li) with shallower acceptor levels [33]. This implies that there is a high density of free holes in the grain interiors of LTNO ceramics. Meanwhile, TiO_2 near the grain boundary also creates some Ni vacancies (V''_{Ni}) as seen in equation (16) [17, 18]. Thus the LTNO system contains a large number of hopping charge carriers (and/or vacancies) and the grain boundary is highly disordered. As previously reported [19], the dielectric permittivity of $Li_{0.10}Ti_xNi_{0.90-x}O$ thin films with 200 nm in thickness increases with increasing Ti content. This result strongly indicates that the Ti dopant in LTNO may not only act as an insulating layer, which obstructs the migration of charge carriers, but may also induce the permanent defect dipoles at the grain boundary. As illustrated in figure 5, the experimental results can be well described by the modified Cole–Cole equation, including the conductivity term. Therefore, the conductivity has contributions to the dielectric permittivity and dielectric loss at low frequency regions, and the dielectric relaxation peaks in higher frequency are associated with permanent dipole orientation or other motions, which do not involve long-range displacement of mobile charge carriers. In general, the grain boundary effect on electric conductivity may originate from a grain boundary potential barrier, which should be ascribed to the thin layer of Ti-rich boundary. As mentioned above, we think that the giant dielectric permittivity response of LTNO (or other dielectric material of co-doped NiO) can be partially contributed from Maxwell–Wagner space charge (long-range migration of carriers) effects at low frequency regions due to the difference of potentials barrier between grain (core) and grain boundary (shell). At high frequency, it is partially contributed from the polarization of highly permanent defect dipoles.

4. Conclusion

The high dielectric permittivity LTNO ceramics have been successfully synthesized by a simple PVA-sol–gel method. XRD results show the single phase of NiO. The temperature and frequency dependence of dielectric permittivity and dielectric loss were investigated. An excellent fit between the experimental and simulated data has been obtained over a wide frequency and temperature using the modified Cole–Cole model with the consideration of the conductivity contribution. The high dielectric permittivity response can be ascribed to the Maxwell–Wagner polarization mechanism and defect-dipole polarization.

Acknowledgments

The authors would like to thank the Department of Physics, Ubon Ratchathani University and the Faculty of Science Electron Microscopy Unit, Khon Kaen University for providing XRD and SEM facilities, respectively. PT and ST would like to thank the National Science and Technology Development Agency (NSTDA) for financial support of their studies through the TGIST and YSTP Programs, respectively. This work was financially supported by the Thailand Research Fund (TRF) and The Commission on Higher Education (CHE), The Ministry of Education, Thailand.

References

[1] Subramanian M A, Li D, Duan N, Reisner B A and Sleight A W 2000 *J. Solid State Chem.* **151** 323
Ramirez A P, Subramanian M A, Gardel M, Blumberg G, Li D, Vogt T and Shapiro S M 2000 *Solid State Commun.* **115** 217
Homes C C, Vogt T, Shapiro S M, Wakimoto S and Ramirez A P 2001 *Science* **293** 673
[2] Raevski I P, Prosandeev S A, Bogatin A S, Malitskaya M A and Jastrabik L 2003 *J. Appl. Phys.* **93** 4130
[3] Abdelkafi Z, Abdelmoula N, Khemakhem H, Bidault O and Maglione M 2006 *J. Appl. Phys.* **100** 114111
[4] Wu J, Nan C W, Lin Y and Deng Y 2002 *Phys. Rev. Lett.* **89** 217601
[5] Maensiri S, Thongbai P and Yamwong T 2007 *Acta Mater.* **55** 2851
[6] Lin Y, Wang J, Jiang L, Chen Y and Nan C W 2004 *Appl. Phys. Lett.* **85** 5664
[7] Lin Y, Jiang L, Zhao R and Nan C W 2005 *Phys. Rev.* B **72** 014103
[8] Jana P K, Sarkar S and Chaudhuri B K 2006 *Appl. Phys. Lett.* **88** 182901
[9] Jana P K, Sarkar S, Sakata H, Watanabe T and Chaudhuri B K 2008 *J. Phys. D: Appl. Phys.* **41** 065403
[10] Hsiao Y J, Change Y S, Fang T H, Chai T L, Chung C Y and Chang Y H 2007 *J. Phys. D: Appl. Phys.* **40** 863
[11] Meansiri S, Thongbai P and Yamwong T 2007 *Appl. Phys. Lett.* **90** 202908
[12] Sinclair D C, Adams T B, Morrison F D and West A R 2002 *Appl. Phys. Lett.* **80** 2153
[13] Cohen M H, Neaton J B, He L and Vanderbilt D 2003 *J. Appl. Phys.* **94** 3299
[14] Lunkenheimer P, Fichtl R, Ebbinghaus S G and Loidl A 2004 *Phys. Rev.* B **70** 172102
[15] Liu J, Duan C, Mei W N, Smith R W and Hardy J R 2005 *J. Appl. Phys.* **98** 093703
[16] Chung S Y, Kim I L D and Kang S J L 2004 *Nat. Mater.* **3** 774
[17] Lin Y H, Li M, Nan C W, Li J, Wu J and He J 2006 *Appl. Phys. Lett.* **89** 032907
[18] Lin Y, Zhao R, Wang J, Cai J, Nan C W, Wang Y and Wei L 2005 *J. Am. Ceram. Soc.* **88** 1808
[19] Zhang Y R, Zhang B P, Dong Y and Li J F 2007 *Key Eng. Mater.* **336–338** 2639
[20] Yamamoto S, Kakihana M and Kato S 2000 *J. Alloys Compounds* **297** 81

[21] Wu J B, Nan J, Nan C W, Lin Y, Deng Y and Zhao S 2003 *Mater. Sci. Eng.* B **99** 294
[22] Terkura K, Williams A R and Oguchi T 1984 *Phys. Rev. Lett.* **52** 1830
[23] Nan C W 1993 *Prog. Mater. Sci.* **37** 1
Waser R and Hagenbeck R 2000 *Acta Mater.* **48** 797
[24] Hence L L and West J K 1990 *Principles of Electronic Ceramics* (New York: Wiley)
[25] Cole K S and Cole R H 1941 *J. Chem. Phys.* **9** 342
[26] Macdonald J R 2005 *Impedance Spectroscopy* (New York: Wiley)
[27] Ming D, Reau J M, Ravez J, Gitae J and Hagenmuller P 1995 *J. Solid State Chem.* **116** 185
[28] Thongbai P, Masingboon1 C, Maensiri S, Yamwong T, Wongsaenmai S and Yimnirun R 2007 *J. Phys.: Condens. Matter* **19** 236208
[29] Moulson A J and Herbert J M 2003 *Electroceramics* (New York: Wiley)
[30] Zhang L and Tang Z J 2004 *Phys. Rev.* B **70** 174306
[31] Li W and Schwartz R W 2006 *Appl. Phys. Lett.* **89** 242906
[32] Leon C, Rivera A, Varez A, Sanz J, Santamaria J and Ngai K L 2001 *Phys. Rev. Lett.* **86** 1279
[33] van Houten S 1960 *J. Phys. Chem. Solids* **17** 7
[34] Lany S, Guillen J O and Zunger A 2007 *Phys. Rev.* B **75** 241203